

Hyperfine Structure of Antiprotonic Helium Revealed by a Laser-Microwave-Laser Resonance Method

E. Widmann,¹ J. Eades,¹ T. Ishikawa,¹ J. Sakaguchi,¹ T. Tasaki,¹ H. Yamaguchi,¹ R. S. Hayano,^{2,*} M. Hori,² H. A. Torii,³
B. Juhász,⁴ D. Horváth,⁵ and T. Yamazaki⁶

¹Department of Physics, University of Tokyo, 7-3-1 Hongo, Bunkyo-ku, Tokyo 113-0033, Japan

²CERN, CH-1211 Geneva 23, Switzerland

³Institute of Physics, University of Tokyo, 3-8-1 Komaba, Meguro-ku, Tokyo 153-8902, Japan

⁴Institute of Nuclear Research of the Hungarian Academy of Sciences, H-4001 Debrecen, Hungary

⁵KFKI Research Institute for Particle and Nuclear Physics, H-1525 Budapest, Hungary

⁶RI Beam Science Laboratory, RIKEN, Wako, Saitama 351-0198, Japan

(Received 13 July 2002; published 22 November 2002)

Using a newly developed laser-microwave-laser resonance method, we observed a pair of microwave transitions between hyperfine levels of the $(n, L) = (37, 35)$ state of antiprotonic helium. This experiment confirms the quadruplet hyperfine structure arising from the interaction of the antiproton orbital angular momentum, the electron spin and the antiproton spin as predicted by Bakalov and Korobov. The measured frequencies of $\nu_{\text{HF}}^+ = 12.895\,96 \pm 0.000\,34$ GHz and $\nu_{\text{HF}}^- = 12.924\,67 \pm 0.000\,29$ GHz agree with recent theoretical calculations on a level of 6×10^{-5} .

DOI: 10.1103/PhysRevLett.89.243402

PACS numbers: 36.10.-k, 32.10.Fn, 33.40.+f

We report the first observation of microwave-induced transitions between magnetic substates of antiprotonic helium and use the results to determine its quadruplet hyperfine splitting to better than 1 MHz (relative precision $\sim 3 \times 10^{-5}$). Antiprotonic helium is an exotic three-body system consisting of a helium nucleus, an antiproton, and an electron ($\bar{p} - e^- - \text{He}^{2+} \equiv \bar{p}\text{He}^+$). It has a series of highly excited metastable states (lifetime $\sim \mu\text{s}$) with principal quantum number n and angular momentum quantum number L in the range 33–39, which have been extensively studied by laser spectroscopy (see [1,2] and a comprehensive review [3]). In the most recent experiments performed at the CERN Antiproton Decelerator (AD), the wavelengths of several laser-induced transitions of the antiproton in $\bar{p}\text{He}^+$ were measured with a relative accuracy of 1.3×10^{-7} , leading to a CPT test limiting any relative difference in the masses and charges of the proton and antiproton to 6×10^{-8} [4]. A step further in the precision spectroscopy of antiprotonic helium is the investigation of its magnetic *hyperfine structure*, i.e., the level splitting caused by the magnetic interaction of the \bar{p} orbital angular momentum $\vec{L}_{\bar{p}}$, the electron spin \vec{S}_e , and the \bar{p} spin $\vec{S}_{\bar{p}}$. To the leading order, the electron in $\bar{p}\text{He}^+$ is in the $1s_{1/2}$ state with a spin magnetic moment $\vec{\mu}_e = g_e \mu_B \vec{S}_e$. The \bar{p} magnetic moment, on the other hand, consists of an orbital part and a spin part $\vec{\mu}_{\bar{p}} = (g_{\ell}^{\bar{p}} \vec{L}_{\bar{p}} + g_s^{\bar{p}} \vec{S}_{\bar{p}}) \mu_{\bar{N}}$. The orbital g factor, $g_{\ell}^{\bar{p}}$, defines the relation between the \bar{p} orbital magnetic moment and the antinuclear magneton $\mu_{\bar{N}} = Q_{\bar{p}} \hbar / (2M_{\bar{p}})$. Its value is usually implicitly taken to be one, but this theoretical relation has never been tested experimentally, either for the proton or the antiproton. Because of the large angular momentum of $\bar{p}\text{He}^+$, the dominant splitting arises from the magnetic interaction of \vec{S}_e with

$\vec{L}_{\bar{p}}$. Thus, the coupling of $\vec{\mu}_{\bar{p}}$ with $\vec{\mu}_e$ creates a doublet [called here *hyperfine (HF)* splitting] with $\vec{F} = \vec{L}_{\bar{p}} + \vec{S}_e$ ($F^- = L - 1/2$ and $F^+ = L + 1/2$). The interaction of the \bar{p} spin magnetic moment with the other magnetic moments splits each sublevel F^+ and F^- into a still finer doublet, and if $\vec{J} = \vec{F} + \vec{S}_{\bar{p}}$ is the total angular momentum, these further sublevels are associated with its components $J^{-+} = F^- + 1/2 = L$, $J^{--} = F^- - 1/2 = L - 1$, $J^{++} = F^+ + 1/2 = L + 1$, and $J^{+-} = F^+ - 1/2 = L$. We refer to this as *superhyperfine (SHF)* splitting.

The theoretical framework of the hyperfine structure of $\bar{p}\text{He}^+$ has been established by Bakalov and Korobov [5] who showed that the SHF splitting resulting from the one-body spin-orbit coupling of the antiproton ($\vec{L}_{\bar{p}} \cdot \vec{S}_{\bar{p}}$), and the scalar ($\vec{S}_{\bar{p}} \cdot \vec{S}_e$) and tensor [$(\vec{S}_{\bar{p}} \cdot \vec{S}_e) - 3(\vec{S}_{\bar{p}} \times \vec{L}_{\bar{p}}) \cdot (\vec{S}_e \times \vec{L}_{\bar{p}}) / [L(L+1)]$] spin-spin couplings, yield the level order as shown in Fig. 1(a) due to an approximate cancellation of the scalar and tensor spin-spin coupling terms. Typical values for the HF splitting of metastable states are $\nu_{\text{HF}} = 10\text{--}15$ GHz, while the SHF splitting is almost 2 orders of magnitude smaller ($\nu_{\text{SHF}}^{\pm} = 150\text{--}300$ MHz). In a previous experiment at the CERN low energy antiproton ring (LEAR) we indeed observed a doublet splitting of the $(n, L) = (37, 35) \rightarrow (38, 34)$ laser transition at $\lambda = 726.1$ nm, the two sublimes being separated by $\Delta = f_+ - f_- = \nu_{\text{HF}}(\text{initial}) - \nu_{\text{HF}}(\text{final}) = 1.75 \pm 0.05$ GHz [6], in agreement with the theoretical value [5]. Although the SHF splitting is too small to be resolved with the pulsed laser system used in our experiments, it causes a small splitting of the hyperfine transition into two components, ν_{HF}^+ and ν_{HF}^- for $J^{-+} \leftrightarrow J^{++}$ and $J^{--} \leftrightarrow J^{+-}$, respectively, as shown in Fig. 1(a). We developed the laser-microwave-laser resonance method

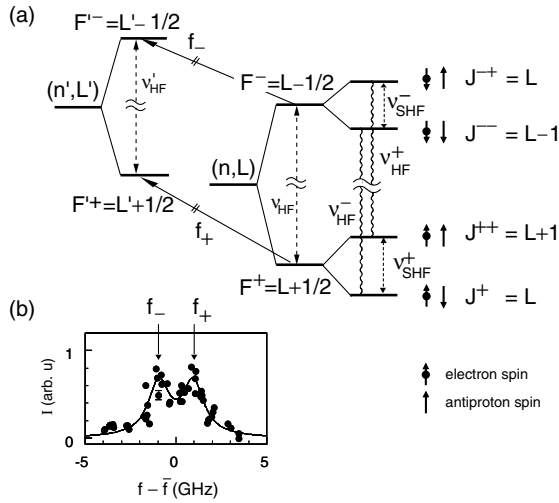


FIG. 1. (a) Schematic view of the splitting of a $\bar{p}\text{He}^+$ state and observable laser transitions from the F^\pm levels of a (n, L) state to a daughter state (n', L') (arrows). Wavy lines denote allowed magnetic transitions associated with an electron spin flip. (b) Laser scan of the 726.1 nm transition with $(n, L) = (37, 35)$ and $(n', L') = (38, 34)$ performed at the AD [$\bar{f} = (f_+ + f_-)/2$].

described below in order to determine ν_{HF}^+ and ν_{HF}^- directly on the MHz level for the case of the $(37, 35)$ state.

The experiment was performed at the antiproton decelerator (AD) of CERN, which delivered pulses of $2-4 \times 10^7 \bar{p}$ of 200 ns length (FWHM) with a momentum of 100 MeV/c (5.3 MeV kinetic energy). One such pulse was extracted from the AD every ~ 2 minutes and stopped in helium gas (see Fig. 2) at a temperature of 6.1 K and pressures of 250 or 530 mbar (number densities 3.0 or $6.7 \times 10^{20} \text{ cm}^{-3}$, respectively). As described in further detail in Ref. [4], the time spectrum of delayed annihilations (ADATS, for analog delayed annihilation time spectrum) was recorded in a digital oscilloscope as the envelope of the output of photomultipliers (PMTs) connected to two Čerenkov counters through which the antiproton annihilation products passed. Because 97% of antiprotons stopped in helium annihilate promptly (within picoseconds), the PMTs were turned off by a gate pulse until ~ 440 ns after the center of the AD pulse.

The wavy lines in Fig. 1(a) represent allowed M1 transitions (flipping \vec{S}_e but not $\vec{S}_{\bar{p}}$) which can be induced by microwave radiation. All the HF levels are initially nearly equally populated. In order to create a population asymmetry which is needed to detect a microwave transition, a laser pulse stimulating a transition from a metastable ($\tau \sim \mu\text{s}$) state to a short-lived ($\tau \lesssim 10$ ns) state can be used. When the \bar{p} is excited to the short-lived state, the $\bar{p}\text{He}^+$ undergoes an Auger transition to a $\bar{p}\text{He}^{2+}$ ion which is immediately destroyed via collisional Stark effect in the dense helium medium followed by annihilation of the \bar{p} with a nucleon. An on-resonance laser pulse therefore superposes a sharp spike onto the ADATS

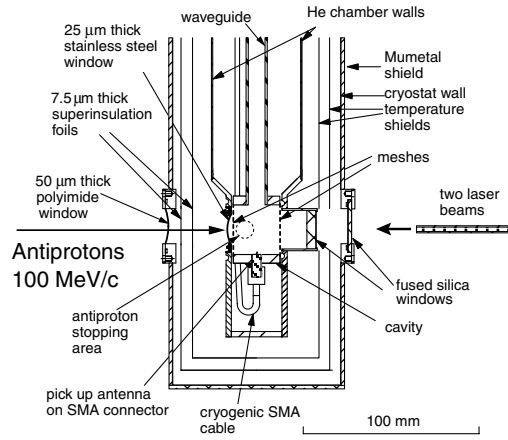


FIG. 2. Side view of the cryostat holding the helium target chamber and microwave cavity. The antiprotons enter the helium chamber from left and stop inside a cylindrical microwave cavity. Two overlapping laser beams come from opposite directions along the cavity cylinder axis, and the microwave radiation is supplied through a rectangular wave guide from the top. Two Čerenkov counters not shown in the drawing were placed on those sides of the cryostat where there is no window.

(cf. Fig. 3) whose area is proportional to the population of the metastable state at the time of the arrival of the laser pulse.

The laser-microwave-laser resonance method utilizes the following sequence: (i) a laser pulse tuned to one of the doublet lines [e.g., f_+ in Fig. 1(a)] preferentially depopulates the F^+ over the F^- doublet. (ii) The microwave pulse is applied; if it is resonant with either ν_{HF}^+ or ν_{HF}^- , it transfers population from the F^- to the F^+ doublet. (iii) A second laser pulse at frequency f_+ measures the new population of F^+ after the microwave pulse.

The laser light of $\lambda = 726.1$ nm was produced by a commercial dye laser pumped by a Nd:YAG laser which

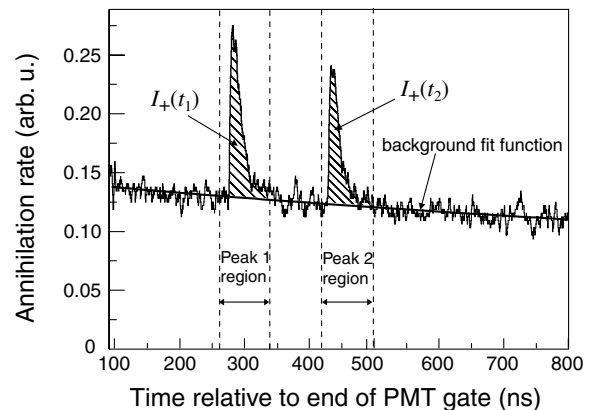


FIG. 3. Part of ADATS with two successively applied laser pulses of frequency f_+ . The background fit function and the two peak regions that are excluded from the background fit are also shown. $I_+(t_1)$ and $I_+(t_2)$ stand for the hatched areas under the two spikes.

was triggered synchronously with the arrival of the anti-proton pulse. The linewidth of the dye laser with intracavity etalon was 0.6–0.8 GHz. A resonance scan [cf. Fig. 1(b)] showed a doublet structure with a separation of $\Delta = f_+ - f_- = 1.8 \pm 0.1$ GHz, in agreement with our earlier observation at LEAR [6]. The two sequential laser pulses were obtained by dividing the output of the dye laser and delaying one part by multiple reflections. In this way a maximum delay of 160 ns could be obtained without seriously degrading the laser beam spot quality.

The Rabi frequency for the allowed microwave transitions averaged over all magnetic sublevels m is given by $\Gamma_{av} = [1/(4\sqrt{2})]g_e\mu_B B_1$, where B_1 is the amplitude of the oscillating magnetic field. From this formula as well as from detailed numerical simulations [7,8] it follows that in order to induce an M1 transition in the 160 ns time difference between the two laser pulses, a B_1 of several gauss is needed. We therefore stopped the antiprotons in a cylindrical cavity immersed in the low-temperature helium gas. This had a central frequency of $\nu_{MW} \sim 12.9$ GHz (diameter 28.8 mm, length 24.6 mm, TM₁₁₀ mode). The ends of the cylinder were covered by metal meshes with a transparency of 85% permitting the \bar{p} and the two laser beams to enter from opposite directions, and the microwave radiation was applied through a rectangular wave guide perpendicular to the cylinder axis. An external triple stub tuner (TST) was used to tune the central frequency and Q value of the cavity, thus allowing the microwave frequency to be scanned over a range of ~ 200 MHz, while keeping Q values of ~ 2700 [8]. The resonance characteristics of the cavity were measured with a vector network analyzer (VNA) both in reflection and in transmission modes. The microwave pulse to induce the electron spin-flip transition was generated by amplifying the VNA output by a pulsed traveling wave tube amplifier (TWTA). For each microwave frequency setting, the ADATS of two Čerenkov counters showing two laser spikes each (cf. Fig. 3) were recorded.

We collected data during five 8 h periods. At the beginning of each period, the laser alignment and depletion efficiency were verified. We then collected approximately 180–290 AD shots, stepping through 10–30 microwave frequencies in cycles. The microwave power was set to the optimum value (15 W) corresponding to an oscillating field strength of $B_1 = 7$ G inside the cavity as obtained from computer simulations. Each cycle included 1–3 points at very low microwave power for use as “microwave-off” reference points.

For each ADATS of one data taking period, we fitted a background function (a sum of two exponentials) to the time spectra in the range from 60 ns after the PMT was turned on to 500 ns after the first laser peak, excluding the two peak regions from the fit as shown in Fig. 3. We extracted the difference between the observed spectrum and the fit function in the two peak windows as shown in Fig. 3. The peak areas $I_+(t_i)$ are proportional to the

population of the F^+ doublet at time t_i . In order to reduce systematic effects such as fluctuations in the overlap of laser and \bar{p} beams or the \bar{p} intensity, which might affect both peaks identically, we calculated the ratio $R^{++} \equiv I_+(t_2)/I_+(t_1)$ and plotted it against ν_{MW} . The individual data sets showed two peaks at the theoretically predicted positions for ν_{HF}^+ and ν_{HF}^- . The off-resonance value of R^{++} agreed with the points taken at extremely low microwave power, but this level varied from data set to data set. This results from uncontrollable systematic effects associated mainly with laser misalignments, which could be compensated in the analysis by normalizing the data sets to their individual “microwave-off” value R_{off}^{++} .

Each data set was then fitted by a sum of two Lorentzian functions with identical width and amplitude, plus a constant background. The results for ν_{HF}^+ and ν_{HF}^- as well as the width of the Lorentzians agreed within the error bars and did not show any dependence on the target density. This is consistent with theoretical arguments presented by Korenman [9] and Bakalov [10] that the shift of the line centers with density is very small, and that the collisional broadening at our densities is at maximum of the order of MHz [9] or as small as 10 kHz [10].

We therefore combined all five data sets and averaged points within 0.7 MHz to give the final spectrum shown in Fig. 4. The measured linewidth $\gamma_{exp} = 5.3 \pm 0.7$ MHz contains the linewidth corresponding to the 160-ns observation time window, $\gamma_{obs} = 1/(2\pi \cdot 160 \text{ ns}) = 1.0$ MHz, the natural width of the (37, 35) state of $\gamma_{(37,35)} = 0.12$ MHz, and other contributions coming either from collisions, the inhomogeneity of the magnetic field over the stopping distribution of \bar{p} , or the fact that the many substates with magnetic quantum numbers $m = -J, \dots, J$ each have different Rabi frequencies.

The final results for ν_{HF}^+ and ν_{HF}^- obtained from fitting two Lorentzians plus a constant background to the spectrum of Fig. 4 are presented in Table I and compared to

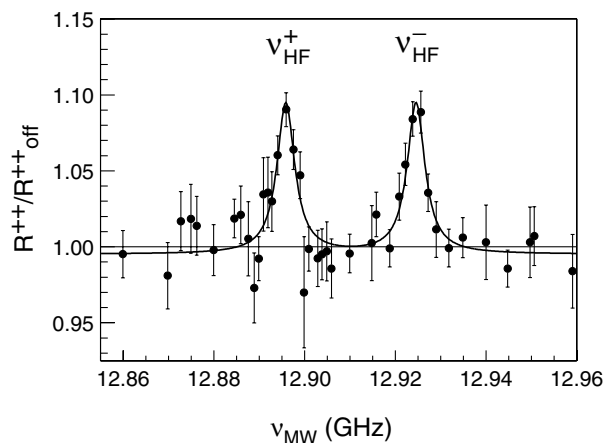


FIG. 4. Average of all microwave scans showing clearly two resonance lines as predicted. The width of the lines of ~ 5 MHz corresponds to 4×10^{-4} of the central frequency.

TABLE I. Experimental values for the HF transition frequencies of the state (37, 35) in GHz compared to theoretical results. The relative experimental error δ_{exp} and the difference $\Delta_{\text{th-exp}} \equiv (\nu_{\text{th}} - \nu_{\text{exp}})/\nu_{\text{exp}}$ are given in ppm.

	ν_{HF}^+ (GHz)	δ_{exp} (ppm)	ν_{HF}^- (GHz)	δ_{exp} (ppm)
Expt.	12.895 96(34)	27	12.924 67(29)	23
		$\Delta_{\text{th-exp}}$		$\Delta_{\text{th-exp}}$
BK [5]	12.895 97	0.6	12.923 94	-57
KB [11]	12.896 346 2	30	12.924 242 8	-33
YK [12]	12.898 977	234	12.926 884	171
K [13]	12.896 073 91	8.6	12.923 963 79	-55

recent theoretical calculations by two groups. The theoretical values for ν_{HF}^+ and ν_{HF}^- distribute over a much wider range (~ 100 ppm) than the laser transition energies (~ 0.1 ppm) calculated by the same groups (see comparison in Ref. [4]), reflecting a higher sensitivity of the hyperfine coupling terms to the details of the wave functions involved. Nevertheless, the experimental values are in excellent agreement with the results of Korobov and Bakalov (both their initial values BK [5] and their most recent ones KB [11]) as well as the latest values of Kino *et al.* (K [13]).

In summary, we have established a laser-microwave-laser resonance method and succeeded in observing two microwave transitions, ν_{HF}^+ and ν_{HF}^- , in antiprotonic helium. The experiment has fully confirmed the presence of a quadruplet structure originating from the hyperfine coupling of $\vec{L}_{\bar{p}}$, \vec{S}_e , and $\vec{S}_{\bar{p}}$, as predicted by Bakalov and Korobov [5]. The agreement of the experimental values ν_{HF}^+ and ν_{HF}^- with the most updated theoretical values KB and K is about 6×10^{-5} or better, on the level of the accuracy of the calculations. These do not include contributions of relative order $\alpha^2 \approx 5 \times 10^{-5}$ or higher. Presently, the experimental error is about 3×10^{-5} , slightly exceeding the theoretical precision. The excellent agreement between experiment and theory proves the validity of the theoretical expressions of Bakalov and Korobov for the HFS of $\bar{p}\text{He}^+$. The microwave resonance frequencies, ν_{HF}^+ and ν_{HF}^- , themselves are primarily related to the dominant \bar{p} orbital magnetic moment $g_{\ell}^{\bar{p}} \vec{L}_{\bar{p}} \mu_{\bar{N}}$. Thus, the agreement between theory and experiment can be interpreted as an experimental proof of $g_{\ell}^{\bar{p}} = 1$ with a relative precision of $\sim 6 \times 10^{-5}$. We note

that no experimental value exists for g_{ℓ}^p for the proton because no atoms with an orbiting proton exist in the world of ordinary matter. On the other hand, the splitting between ν_{HF}^+ and ν_{HF}^- is caused by the \bar{p} spin magnetic moment, and is directly proportional to $g_{\ell}^{\bar{p}}$. The observation of a splitting in agreement with the theoretical value implies that $g_{\ell}^{\bar{p}} = g_{\ell}^p$ within the experimental error of 1.6%. This is consistent with an earlier (more precise) determination of $g_{\ell}^{\bar{p}}$ from a fine structure measurement of antiprotonic lead [14].

We thank Dr. Fritz Caspers (PS Division, CERN) for invaluable help in the design of the microwave cavity and circuits as well as D. Bakalov, V. I. Korobov, Y. Kino, and N. Yamanaka for many helpful discussions and for providing us with their results prior to publication. The support by the CERN cryogenic laboratory as well as the help of Mr. K. Suzuki and Dr. H. Gilg is acknowledged. The work was supported by the Grant-in-Aid for Creative Basic Research (10NP0101) of Monbukagakusho of Japan, the Hungarian Scientific Research Fund (OTKA T033079 and TeT-Jap-4/02), and the Japan Society for the Promotion of Science.

*On leave from Department of Physics, University of Tokyo, 7-3-1 Hongo, Bunkyo-ku, Tokyo 113-0033, Japan.

- [1] M. Iwasaki *et al.*, Phys. Rev. Lett. **67**, 1246 (1991).
- [2] T. Yamazaki *et al.*, Nature (London) **361**, 238 (1993).
- [3] T. Yamazaki, N. Morita, R. S. Hayano, E. Widmann, and J. Eades, Phys. Rep. **366**, 183 (2002).
- [4] M. Hori *et al.*, Phys. Rev. Lett. **87**, 093401 (2001).
- [5] D. Bakalov and V. I. Korobov, Phys. Rev. A **57**, 1662 (1998).
- [6] E. Widmann *et al.*, Phys. Lett. B **404**, 15 (1997).
- [7] J. Sakaguchi, Master's thesis, University of Tokyo, 2000.
- [8] J. Sakaguchi *et al.* (unpublished).
- [9] G. Ya. Korenman (private communication).
- [10] D. Bakalov (private communication).
- [11] V. Korobov and D. Bakalov, J. Phys. B **34**, L519 (2001).
- [12] N. Yamanaka, Y. Kino, H. Kudo, and M. Kamimura, Phys. Rev. A **63**, 012518 (2001).
- [13] Y. Kino, N. Yamanaka, M. Kamimura, and H. Kudo, in Proceedings of the 3rd European Conference on Atomic Physics at Accelerators (APAC2001), Aarhus, Denmark, 2001 [Hyperfine Interact. (to be published)].
- [14] A. Kreissl *et al.*, Z. Phys. C **37**, 557 (1988).